Front. Phys. 12(5), 126701 (2017)
DOI 10.1007/s11467-017-0681-y

RESEARCH ARTICLE

Fulde–Ferrell–Larkin–Ovchinnikov pairing states between s- and p-orbital fermions

Shu-Yang Wang[1], **Jing-Wei Jiang**[1], **Yue-Ran Shi**[2], **Qiongyi He**[1,3,4], **Qihuang Gong**[1,3,4], **Wei Zhang**[2,5,†]

[1] *State Key Laboratory of Mesoscopic Physics, School of Physics, Peking University, Beijing 100871, China*
[2] *Department of Physics, Renmin University of China, Beijing 100872, China*
[3] *Collaborative Innovation Center of Quantum Matter, Beijing 100871, China*
[4] *Collaborative Innovation Center of Extreme Optics, Shanxi University, Taiyuan 030006, China*
[5] *Beijing Key Laboratory of Opto-electronic Functional Materials and Micro-nano Devices, Renmin University of China, Beijing 100872, China*
Corresponding author. E-mail: †*wzhangl@ruc.edu.cn*
Received December 31, 2016; accepted March 20, 2017

We study the pairing states in a largely imbalanced two-component Fermi gas loaded in an anisotropic two-dimensional optical lattice, where the spin-up and spin-down fermions are filled to the s- and p_x-orbital bands, respectively. We show that owing to the relative inversion of the band structures of the s and p_x orbitals, the system favors pairing between two fermions on the same side of the Brillouin zone, leading to a large stable regime for states with a finite center-of-mass momentum, i.e., the Fulde–Ferrell–Larkin–Ovchinnikov (FFLO) state. In particular, when two Fermi surfaces are close in momentum space, a nesting effect stabilizes a special type of π-FFLO phase with a spatial modulation of π along the easily tunneled x direction. We map out the zero-temperature phase diagrams within the mean-field approach for various aspect ratios within the two-dimensional plane and calculate the Berezinskii–Kosterlitz–Thouless (BKT) transition temperatures T_{BKT} for different phases.

Keywords ultracold Fermi gas, superfluid, optical lattice

PACS numbers 67.85.Lm, 03.75.Ss, 05.30.Fk

1 Introduction

The pairing between fermions residing on separate Fermi surfaces is one of the central questions in the fields of superconductors in a variety of solid-state systems [1], color superconductivity in quark matter [2], and superfluidity in ultracold atomic gases [3]. As was first intrigued by the study of the magnetic-field effect on superconductivity, the discussion of this interesting topic has led to proposals of various exotic pairing states, including the Fulde–Ferrell–Larkin–Ovchinnikov (FFLO) [4, 5], breached pair [6], and deformed Fermi surface phases [7, 8]. Among these candidates, the FFLO state consists of pairs formed by two fermions on top of each individual Fermi surface and is characterized by a finite center-of-mass momentum. Thanks to the high controllability and the separation of charge and spin degrees of freedom, ultracold atomic gases provide a versatile platform to study pairing physics with mismatched Fermi surfaces. A large number of investigations, both experimental and theoretical, suggest that although the FFLO state may be restricted within a narrow parameter regime for a three-dimensional two-component Fermi gas with mismatched Fermi surfaces [9], its existence is favored in low dimensions [10, 11] and in systems with synthetic spin–orbit coupling [12, 13], where the fluctuations in the order parameter wave vector are restricted by the reduction in symmetry.

In addition to Fermi gases confined in harmonic traps, pairing with mismatched Fermi surfaces has also been analyzed theoretically for fermions loaded in optical lattices [14, 15]. One important finding is that owing to the nesting effect between the two Fermi surfaces, either in the s-orbital [14] or in the p-orbital [15] bands, the FFLO state can be remarkably favored as the nest-

*arXiv: 1612.01709v1.

© Higher Education Press and Springer-Verlag Berlin Heidelberg 2017

ing condition is satisfied. This effect is eminent in two dimensions where a van Hove singularity emerges when the nesting is perfect. Moreover, recent studies suggest that when pairing takes place between fermions residing on different orbital bands, a special π-FFLO phase with a center-of-mass momentum $q = \pi/d$ can be stabilized in a large parameter regime for a quasi-one-dimensional (quasi-1D) lattice potential with a lattice spacing d [16–18]. The emergence of such an exotic state is also a result of the nesting effect induced by the relative inversion of the single-particle band structures of the two spin components. This π-FFLO phase, or equivalently referred as the π phase, has been studied in heterostructures of ferromagnetic and superconducting layers [19], high T_c superconductors [20–22], and spin-dependent quasi-1D optical lattices [23] and has potential application for quantum computing in building up superconducting qubits via the π junctions [24, 25]. With the ability to prepare and investigate cold atomic gases in high orbital bands in optical lattices [26–28], it is of interest to extend our understanding of exotic pairing states involving fermions in different orbitals.

In this work, we study the interband pairing within two-component fermions loaded in a two-dimensional (2D) optical lattice. We show that a π-FFLO phase can be stabilized owing to the nesting effect between the s- and p-orbital bands. By employing a mean-field approach, we map out the zero-temperature phase diagram by varying the chemical potential of each spin component and find that the FFLO states, either the π phase or the Fulde–Ferrell (FF) state with a single center-of-mass momentum, are favored within a large parameter window. As a comparison, the Bardeen–Cooper–Schrieffer (BCS) state with a zero center-of-mass pairing momentum is not stable under the mean-field level calculation. We also study the evolution of phase diagrams by reducing the hopping integral along one direction and recover the result for 1D configurations. We then take into account the phase fluctuation on top of the mean-field order parameter and obtain the Berezinskii–Kosterlitz–Thouless (BKT) transition temperature $T_{\rm BKT}$ for the π-FFLO, conventional FF, and the BCS phases.

The remainder of this paper is organized as follows. In Section 2, we present the model under consideration and the mean-field formalism. By minimizing the mean-field thermodynamic potential, we discuss the zero-temperature phase diagrams for various lattice configurations in Section3. The various phases in the phase diagram can be distinguished from their corresponding quasimomentum distributions, which can be extracted using spin-selective time-of-flight imaging and band mapping techniques. We then include the phase fluctuations and obtain the BKT transition temperature in Section 4. Finally, we summarize the main findings in Section 5.

2 Model

We consider a two-component Fermi gas loaded in a quasi-two-dimensional (quasi-2D) cubic optical lattice. The Hamiltonian is

$$H = \int \mathrm{d}^3\boldsymbol{r} \sum_{\sigma=\uparrow,\downarrow} \psi_\sigma^\dagger(\boldsymbol{r}) \left[-\frac{\hbar^2}{2m}\nabla^2 + V_{\rm ol}(\boldsymbol{r}) - \mu_\sigma\right] \psi_\sigma(\boldsymbol{r}) + g\int \mathrm{d}^3\boldsymbol{r}\psi_\uparrow^\dagger(\boldsymbol{r})\psi_\downarrow^\dagger(\boldsymbol{r})\psi_\downarrow(\boldsymbol{r})\psi_\uparrow(\boldsymbol{r}), \quad (1)$$

where $\psi_\sigma^\dagger(\boldsymbol{r})$ and $\psi_\sigma(\boldsymbol{r})$ are the creation and annihilation operators for fermions at the position $\boldsymbol{r}$ having a spin σ, $V_{\rm ol} = \sum_{i=x,y,z} V_{0i}\sin^2(\pi r_i/d)$ is the lattice potential, μ_σ is the chemical potential for σ, and g is the strength for a contact interaction. In the following discussion, we focus on an anisotropic configuration in which V_{0z} is much greater than V_{0y} and V_{0x}, such that the hopping integral along the z direction is negligible to ensure quasi-two-dimensionality. Moreover, we also focus on the case where $V_{0y} > V_{0x}$. This in-plane anisotropy breaks the C_4 rotational symmetry and lifts the degeneracy between the p_x and p_y orbitals so that we can concentrate on the energetically favorable p_x orbital only. We may then refer to the p_x orbital simply as the p orbital to simplify the notation unless specified.

Under the condition of a large population imbalance such that the spin-up fermions are filled to the s orbital while the spin-down particles are filled to the p band, pairing will take place between particles residing on the Fermi surfaces in the s and p bands, as schematically illustrated in Fig. 1. A minimal 2D Hamiltonian involves only these two relevant bands and takes the following form under the tight-binding approximation:

$$H_{\rm 2D} = \sum_{\boldsymbol{k},\sigma}(\epsilon_{\boldsymbol{k},\sigma} - \mu_\sigma)c_{\boldsymbol{k},\sigma}^\dagger c_{\boldsymbol{k},\sigma} + U\sum_{\boldsymbol{k},\boldsymbol{k}',\boldsymbol{q}} c_{\boldsymbol{k}+\boldsymbol{q},\uparrow}^\dagger c_{-\boldsymbol{k}+\boldsymbol{q},\downarrow}^\dagger c_{-\boldsymbol{k}'+\boldsymbol{q},\downarrow} c_{\boldsymbol{k}'+\boldsymbol{q},\uparrow}. \quad (2)$$

Here, we have integrated out the degrees of freedom along the strongly confined z direction. The single-particle dispersion is

$$\epsilon_{\boldsymbol{k},\sigma} = 2J_{x\sigma}(1-\cos k_x) + 2J_{y\sigma}(1-\cos k_y) \quad (3)$$

with the hopping integrals $J_{x\uparrow}, J_{y\uparrow}, J_{y\downarrow} > 0$, and $J_{x\downarrow} < 0$, reflecting the symmetries of the s- and p_x-orbitals for spin-up and spin-down particles, respectively. The specific values of the hopping coefficients are determined by the overlap of the Wannier functions of the corresponding bands at adjacent sites. The on-site interaction U is also obtained by the density–density overlap of the on-site Wannier functions and can be tuned by either changing g via a Feshbach resonance or by varying the

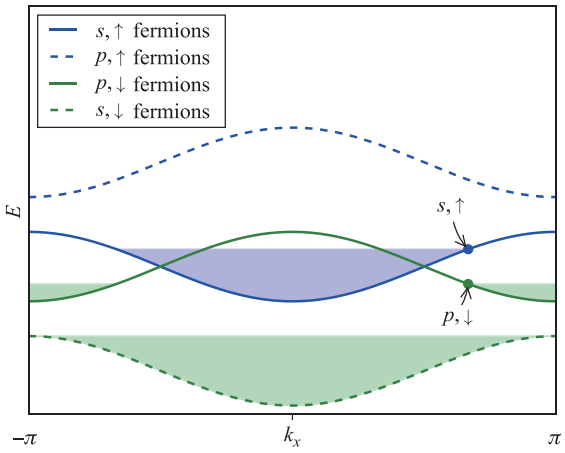

Fig. 1 Schematic of the band occupation for spin-up (blue) and spin-down (green) particles. The spin-down fermions in the s band (dashed green) are inert owing to a large band gap. Pairing takes place between the spin-up fermions in the s band (solid blue) and the spin-down fermions in the p band (solid green). As the dispersions of the s and p bands have opposite curvatures, the system favors pairing between two particles on the same side of the Brillouin zone, leading to a pairing state with a finite center-of-mass momentum.

z-direction lattice depth through a confinement-induced resonance [29–32].

We consider pairing states with one single center-of-mass momentum, i.e., the FF state with the order parameter ansatz $\Delta_{2\boldsymbol{q}} \equiv U \sum_{\boldsymbol{k}} c_{-\boldsymbol{k}+\boldsymbol{q},\downarrow} c_{\boldsymbol{k}+\boldsymbol{q},\uparrow}$. The mean-field Hamiltonian can be written as

$$H_{\mathrm{MF}} = -\frac{|\Delta_{2\boldsymbol{q}}|^2}{U} + \sum_{\boldsymbol{k}} \Big(\xi_{\boldsymbol{k},\uparrow} c^{\dagger}_{\boldsymbol{k},\uparrow} c_{\boldsymbol{k},\uparrow} + \xi_{\boldsymbol{k},\uparrow} c^{\dagger}_{\boldsymbol{k},\uparrow} c_{\boldsymbol{k},\uparrow} + \Delta_{2\boldsymbol{q}} c^{\dagger}_{\boldsymbol{k}+\boldsymbol{q},\uparrow} c^{\dagger}_{-\boldsymbol{k}+\boldsymbol{q},\downarrow} + \Delta^{\dagger}_{2\boldsymbol{q}} c_{-\boldsymbol{k}+\boldsymbol{q},\downarrow} c_{\boldsymbol{k}+\boldsymbol{q},\uparrow} \Big), \quad (4)$$

where $\xi_{\boldsymbol{k},\sigma} = \epsilon_{\boldsymbol{k},\sigma} - \mu_\sigma$. Integrating out the fermionic degrees of freedom, we obtain the thermodynamic potential

$$\Omega = -\frac{|\Delta_{2\boldsymbol{q}}|^2}{U} + \sum_{\boldsymbol{k}} \Big[\xi_{-\boldsymbol{k}+\boldsymbol{q},\downarrow} - \frac{1}{\beta} \ln \big((1 + \mathrm{e}^{-\beta E_{\boldsymbol{k},\boldsymbol{q},+}})(1 + \mathrm{e}^{-\beta E_{\boldsymbol{k},\boldsymbol{q},-}}) \big) \Big], \quad (5)$$

where $\beta = 1/k_B T$ is the inverse temperature, and the two branches of quasiparticle dispersions are given by

$$E_{\boldsymbol{k},\boldsymbol{q},\pm} = \frac{\xi_{\boldsymbol{k}+\boldsymbol{q},\uparrow} - \xi_{-\boldsymbol{k}+\boldsymbol{q},\downarrow}}{2} \pm \sqrt{\left(\frac{\xi_{\boldsymbol{k}+\boldsymbol{q},\uparrow} + \xi_{-\boldsymbol{k}+\boldsymbol{q},\downarrow}}{2} \right)^2 + |\Delta_{2\boldsymbol{q}}|^2}. \quad (6)$$

The ground state of the system can then be determined by minimizing the thermodynamic potential as a function of the amplitude $\Delta \equiv |\Delta_{2\boldsymbol{q}}|$ and the wave vector $\boldsymbol{q}$ of the order parameter while the chemical potentials $\mu_\uparrow$ and $\mu_\downarrow$ are fixed. To ensure mechanical stability, we further calculate the determinant of the compressibility matrix associated with the stable solutions obtained and confirm that all solutions are stable with a positive-definite compressibility matrix.

3 Zero-temperature phase diagrams

We first consider the 1D case with $J_{y\sigma} = 0$. This configuration has been analyzed in previous works using the mean-field approach and density matrix renormalization group method [16, 18], which both suggest large parameter windows for the π-FFLO and conventional FF states. These findings can be understood by noticing that the s- and p-orbital bands have opposite curvatures, such that the Fermi sea for the s band is located at the center of the first Brillouin zone while the p-band Fermi sea lies at the boundary (see Fig. 1). Thus, a pairing state between fermions on different sides of the Brillouin zone can only involve very few particles right on the Fermi surfaces. If one moves slightly below the Fermi surfaces, the center-of-mass momentum of the pairing state has to be modified because the two dispersion curves move in the same direction. For an FF state between fermions on the same side of the Brillouin zone, however, there exist particles available for pairing below the Fermi surfaces. In particular, if the dispersions for the two spin states have analogous curvatures, a nesting effect can significantly enhance the pairing instability due to the increase in the density of states. We emphasize that the pairing mechanism mentioned above originates from the different topologies of s- and p-orbital bands and not the Fermi-surface mismatch as in a superconductor with a magnetization [4, 5].

In Fig. 2(a), we show the mean-field phase diagram by varying the chemical potentials of the two spin species. We choose the hopping integral for spin up along the x direction to be the energy unit $J_{x\uparrow} = J = 1$ and set $J_{x\downarrow} = -1$ to accommodate the symmetry of the p-orbital band. In Fig. 2, we define the average chemical potential μ_{aver} and the chemical potential difference $\delta\mu$ as

$$\mu_{\mathrm{aver}} = \frac{\mu_\uparrow + \mu_\downarrow}{2}, \qquad \delta\mu = \mu_\uparrow - \mu_\downarrow. \quad (7)$$

Note that the single-particle dispersions for spin-up and spin-down fermions range within $\epsilon_{\boldsymbol{k},\uparrow}/J \in [0, 4]$ and $\epsilon_{\boldsymbol{k},\downarrow}/J \in [-4, 0]$, respectively. As the s- and p-orbital bands are symmetric under reflection for this special choice of parameters, the phase diagram is also symmetric along $\mu_{\mathrm{aver}}/J = 0$ and $\delta\mu/J = 4$. We emphasize that under the local density approximation (LDA) while assuming both spin species experience the same global

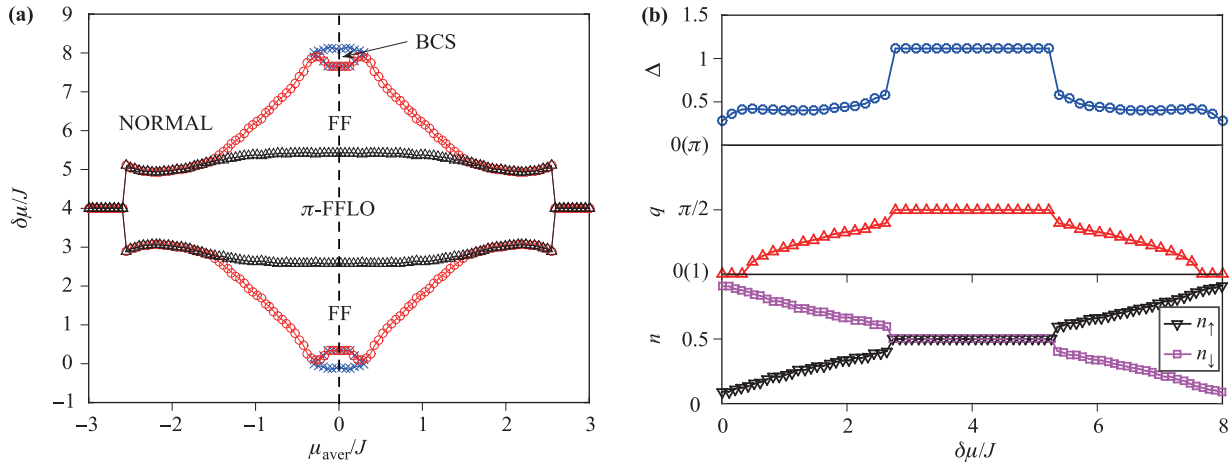

Fig. 2 **(a)** Phase diagram of a one-dimensional configuration with $J_{y\sigma}/J = 0$ by varying the average chemical potential $\mu_{\rm aver}$ and chemical potential difference $\delta\mu$. The π-FFLO phase is characterized by a center-of-mass momentum of $qd = \pi/2$. **(b)** Variations in Δ, q, and the number densities by changing $\delta\mu$ with $\mu_{\rm aver}/J = 0$ when moving along the dashed line in the phase diagram in (a). The π-FFLO–FF and BCS–Normal phase transitions are of the first order, whereas the FFLO–BCS transition is of the second order. Other parameters used here are $J_{x\uparrow}/J = 1$, $J_{x\downarrow}/J = -1$, and $U/J = -3.3$.

trapping potential, a horizontal line in such a phase diagram represents a trajectory from a trap center to its edge with the average chemical potential at the trap center fixed by that at the starting point of the line.

One striking feature of this phase diagram is a large stable region for the π-FFLO state, which is characterized by a finite order parameter amplitude Δ and a center-of-mass momentum $2qd/\pi$, as illustrated in Fig. 2(b). Note that the π-FFLO phase is present near the regime $\delta\mu/J \sim 4$, where the Fermi surfaces for the two spin species are close in the first Brillouin zone. This observation is consistent with the understanding of the pairing mechanism for the π-FFLO state, i.e., the nesting effect between the two Fermi surfaces connected by $2\pi/d$. When the chemical potential difference $\delta\mu/J$ is moved further away from 4, the nesting condition for the two Fermi surfaces is no longer a momentum shift of $2\pi/d$. In this case, the π-FFLO phase becomes energetically unfavorable compared to a conventional FF state, which processes the correct center-of-momentum $2q$ for nesting. The transition between the π-FFLO and conventional FF phases is of the first order, as shown in Fig. 2(b). As the number densities for both spins feature abrupt changes at the phase boundaries, a phase separation regime would emerge in phase diagrams for a uniform system with fixed number densities. Finally, we also identify a small BCS regime around $\mu_{\rm aver}/J \approx 0$ and $\delta\mu/J \approx 0$ or 8. These regimes correspond to the condition that the band of one spin species is almost completely filled while the other is nearly empty so that pairing takes place between two fermions either residing near the center or the opposite boundaries of the first Brillouin zone, leading to a pairing state with a zero center-of-mass momentum. The BCS-FF phase boundary is of the second order, as suggested by the smooth variations in Δ and q shown in Fig. 2(b).

With the understanding of the 1D phase diagram and the properties of the various phases therein, we next discuss a 2D configuration with $J_{y\uparrow}/J \neq 0$. We remind the reader that we only consider an anisotropic 2D lattice that has a higher lattice potential along the y direction than that along the x direction, such that we only need to take the lowest lying p_x orbital into consideration. Thus, the hopping integral for spin-down atoms lying in the p_x orbital is strongly anisotropic with $J_{y\downarrow}/J \ll 1$. In Figs. 3(a) and (b), we assume $J_{y\downarrow} = 0$ and show the zero-temperature phase diagrams for $J_{y\uparrow}/J = 0.1$ and 0.5, respectively. We find that the general structure of the phase diagrams is similar to that for one dimension. Specifically, there is a large region in which the π-FFLO phase is stable. The center-of-mass wave vector for this state is $2\boldsymbol{q} = (\pi/d, 0)$. The π-FFLO phase is surrounded by a conventional FF phase characterized by the wave vector $2\boldsymbol{q} = (2q_x, 0)$ via a first-order phase transition.

There are, however, some distinct features present in the 2D case, in particular for large $J_{y\uparrow}/J$, as shown in Fig. 3(b). First, the stable region for the FF state is significantly extended when the chemical potentials satisfy a certain condition, as depicted by the dashed line in Fig. 3(b). Along this line, the two Fermi surfaces of different spin species can have some nesting, leading to an enlarged density of states and hence a pairing instability. Second, the BCS state disappears with increasing $J_{y\uparrow}/J$. This is also a consequence of the enhanced FF instability induced by the 2D nesting condition.

The transition between the π-FFLO and conventional

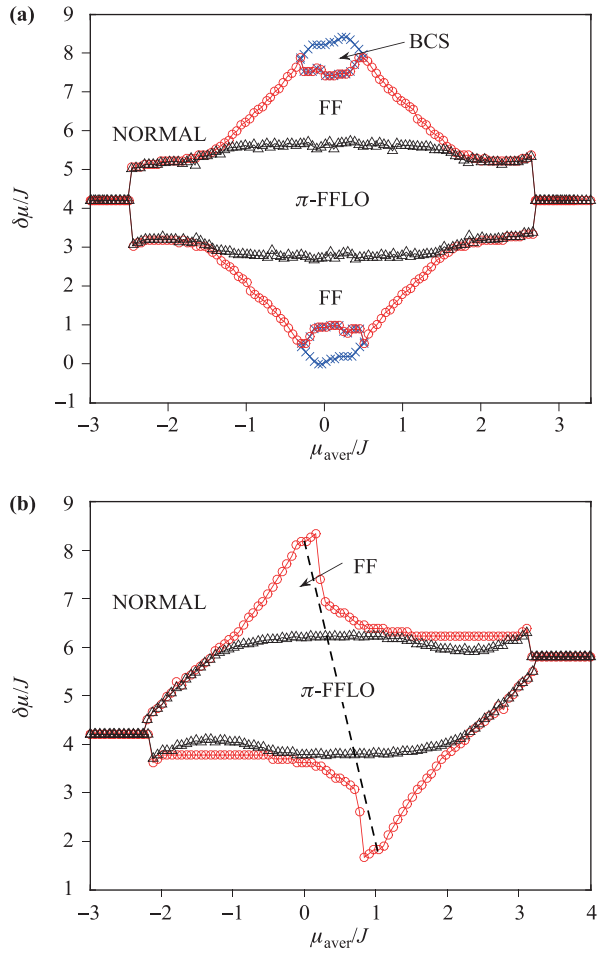

Fig. 3 Phase diagram for a two-dimensional system with **(a)** $J_{y\uparrow}/J = 0.1$ and **(b)** $J_{y\uparrow}/J = 0.5$. The hopping integral for spin-down atoms along the y axis $J_{y\downarrow}/J = 0$, reflecting the strong anisotropy of the p_x orbital. Other parameters are the same as in Fig. 2.

FF states can be identified by the momentum distribution of the particles in the first Brillouin zone. As can be seen from Fig. 4, the density profile of the spin-up particles in the quasimomentum space features abrupt changes after passing the transition line from the π-FFLO (left column) state to the conventional FF (right column) state for both cases of $J_{y\uparrow}/J = 0.1$ (top row) and $J_{y\uparrow}/J = 0.5$ (bottom row). The momentum distributions can be obtained by band mapping spin-selective time-of-flight images.

4 Superfluid transition temperature

In this section, we consider the phase fluctuations around the mean-field order parameter by studying $\Delta_{2\boldsymbol{q}} = |\Delta| + |\delta\Delta|\mathrm{e}^{\mathrm{i}\theta}$, where $|\delta\Delta|$ and θ are the amplitude and phase of the fluctuations [33]. By substituting the expression

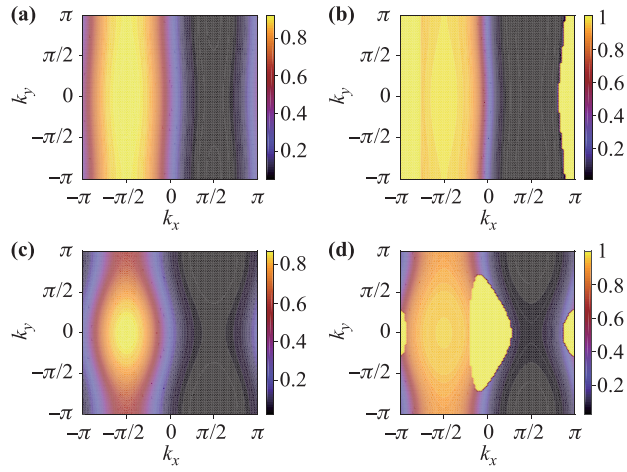

Fig. 4 Density distribution of spin-up atoms in the first Brillouin zone. Plots in the top row correspond to cases where $J_{y\uparrow}/J = 0.1$ with $\mu_{\mathrm{aver}}/J = 0$ and **(a)** $\delta_\mu/J = 5.5$ and **(b)** $\delta_\mu/J = 5.7$, whereas those in the bottom row correspond to cases where $J_{y\uparrow}/J = 0.5$ with $\mu_{\mathrm{aver}}/J = 0$ and **(c)** $\delta_\mu/J = 6.2$ and **(d)** $\delta_\mu/J = 6.4$. When passing from the π-FFLO state (left column) to the FF state (right column), the density distribution $n_\uparrow(\boldsymbol{k})$ shows a clear signature that can be identified by band mapping time-of-flight images. Other parameters are the same as in Fig. 3.

above into the thermodynamic potential in Eq. (5) and integrating out the amplitudes, we obtain the superfluid density

$$\rho_{ij} = \frac{m}{\hbar^2}\left(\frac{\partial^2\Omega}{\partial q_{si}\partial q_{sj}}\right)\bigg|_{\boldsymbol{q}_s=0}, \tag{8}$$

where $\boldsymbol{q}_s = (q_{sx}, q_{sy}) \equiv (\partial_x\theta, \partial_y\theta)$ is the wave vector associated with the superfluid velocity. Note that the superfluid density is a tensor for the most general case with anisotropy. The diagonal elements are

$$\begin{aligned}\rho_{xx} = \frac{m}{\hbar^2}\sum_{\boldsymbol{k},\eta=\pm}\Bigg[&\left(c_{x-} + \eta\frac{\xi c_{x+} + \frac{\Delta^2}{\xi^2+\Delta^2}s_{x+}^2}{\sqrt{\xi^2+\Delta^2}}\right)f(E_\eta)\\ &-\frac{\beta}{4}\left(s_{x-} + \eta\frac{\xi}{\sqrt{\xi^2+\Delta^2}}s_{x+}\right)^2\mathrm{sech}^2\frac{\beta E_\eta}{2}\Bigg],\\ \rho_{yy} = \frac{m}{\hbar^2}\sum_{\boldsymbol{k},\eta=\pm}\Bigg[&\left(c_{y-} + \eta\frac{\xi c_{y+} + \frac{\Delta^2}{\xi^2+\Delta^2}s_{y+}^2}{\sqrt{\xi^2+\Delta^2}}\right)f(E_\eta)\\ &-\frac{\beta}{4}\left(s_{y-} + \eta\frac{\xi}{\sqrt{\xi^2+\Delta^2}}s_{y+}\right)^2\mathrm{sech}^2\frac{\beta E_\eta}{2}\Bigg].\end{aligned} \tag{9}$$

In the expressions above, $f(x) = 1/(1+\mathrm{e}^{\beta x})$ is the Fermi distribution function, $\xi = (\xi_{\boldsymbol{k}+\boldsymbol{q},\uparrow} + \xi_{-\boldsymbol{k}+\boldsymbol{q},\downarrow})/2$, and

$$\begin{aligned} s_{\sigma\pm} &= J_{\sigma\uparrow}\sin(k_\sigma + q_\sigma) \pm J_{\sigma\downarrow}\sin(-k_\sigma + q_\sigma),\\ c_{\sigma\pm} &= J_{\sigma\uparrow}\cos(k_\sigma + q_\sigma) \pm J_{\sigma\downarrow}\cos(-k_\sigma + q_\sigma). \end{aligned} \tag{10}$$

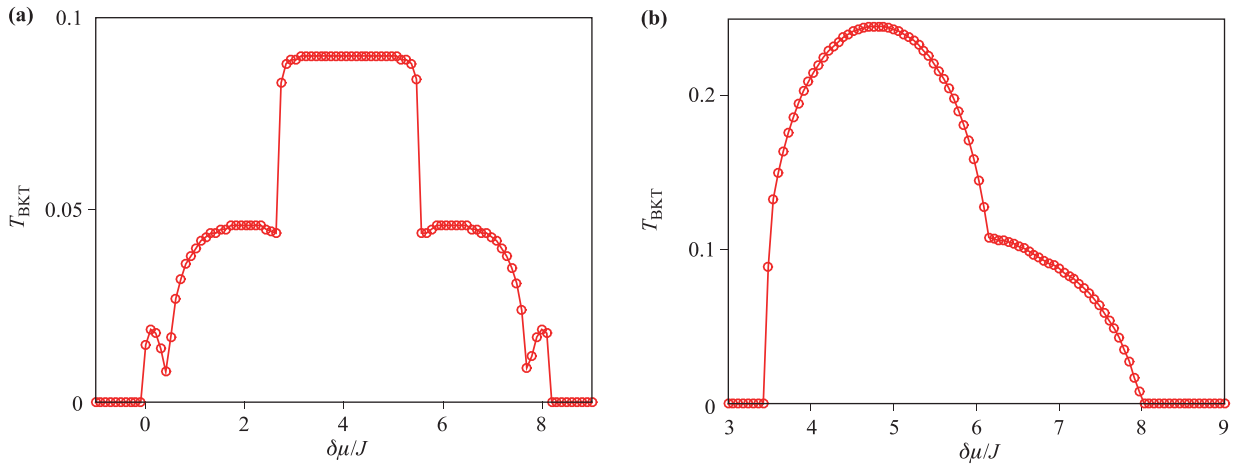

Fig. 5 Superfluid transition temperature $T_{\rm BKT}$ for **(a)** $J_{y\uparrow}/J = 0.1$ and $J_{y\downarrow}/J = 0.05$ and **(b)** $J_{y\uparrow}/J = 0.5$ and $J_{y\downarrow}/J = 0.1$. Note that the BCS state acquires an elevated transition temperature due to the increase in the superfluid density. The average chemical potential $\mu_{\rm aver}/J = 0$ and other parameters are the same as in Fig. 2.

In two dimensions, the superfluid transition temperature is the BKT type [34, 35], which is associated with the association and dissociation of vortex and antivortex pairs. The equation for the BKT temperature $T_c = T_{\rm BKT}$ is determined by the Kosterlitz–Thouless condition [35]

$$T_{\rm BKT} = \frac{\pi}{2}\sqrt{\rho_{xx}\rho_{yy}}. \tag{11}$$

This equation must be solved self-consistently with the minimization condition for the thermodynamic potential in Eq. (5) to determine Δ, $\boldsymbol{q}$, and $T_{\rm BKT}$.

The solutions for $T_{\rm BKT}$ are shown in Fig. 5. Note that rather than assuming $J_{y\downarrow}/J = 0$ as in Section 3, we consider a small but finite $J_{y\downarrow}/J$ here to ensure that the system is two-dimensional in nature. For the strongly anisotropic case with $J_{y\uparrow}/J = 0.1$ and $J_{y\downarrow}/J = 0.05$, as shown in Fig. 5(a), the critical temperature reaches its maximum at the center of the π-FFLO regime, where the two bands are both half-filled such that the nesting is strong. As the two Fermi surfaces deviate from this optimistic condition, $T_{\rm BKT}$ is reduced to lower values and features an abrupt drop when entering the FF regime. Interestingly, the BCS state located in the region with most separated Fermi surfaces acquires a slightly elevated critical temperature. As the system crosses from 1D to 2D with $J_{y\uparrow}/J = 0.5$ and $J_{y\downarrow}/J = 0.1$ [Fig. 5(b)], a highest transition temperature is also achieved when the two bands are both half-filled.

5 Conclusion

We investigate the interband pairing in an anisotropic two-dimensional optical lattice when the Fermi surface of one spin species is located in the s band and the other in the p_x-orbital band. By mapping the zero-temperature phase diagrams, we conclude that FF pairing states with a finite center-of-mass momentum are favored in a large parameter window owing to the relative inversion of the band structures and the nesting effect. Specifically, a π-FFLO state with a spatial modulation of two times the lattice spacing along the easily tunneled x direction can be stabilized when the Fermi surfaces for the two spin species are close within the Brillouin zone. We further discuss the fluctuation effect at finite temperatures and calculate the BKT transition temperature for various phases.

Acknowledgements This work was supported by the National Natural Science Foundation of China (Grant Nos. 11274009, 11274025, 11434011, 11522436, 11622428, 61475006, and 61675007), the National Key R&D Program (Grant Nos. 2013CB922000 and 2016YFA0301201), the Ministry of Science and Technology of China (Grant No. 2016YFA0301302), and the Research Funds of Renmin University of China (Grant Nos. 10XNL016 and 16XNLQ03).

References

1. R. Casalbuoni and G. Nardulli, Inhomogeneous superconductivity in condensed matter and QCD, *Rev. Mod. Phys.* 76(1), 263 (2004)
2. M. Alford, J. A. Bowers, and K. Rajagopal, Crystalline color superconductivity, *Phys. Rev. D* 63(7), 074016 (2001)
3. Y. A. Liao, A. S. C. Rittner, T. Paprotta, W. Li, G. B. Partridge, R. G. Hulet, S. K. Baur, and E. J. Mueller, Spin-imbalance in a one-dimensional Fermi gas, *Nature* 467(7315), 567 (2010)
4. P. Fulde and R. A. Ferrell, Superconductivity in a strong spin-exchange field, *Phys. Rev.* 135(3A), A550 (1964)

5. A. I. Larkin and Y. N. Ovchinnikov, Nonuniform state of superconductors, *Sov. Phys. JETP* 20, 762 (1965)
6. W. V. Liu and F. Wilczek, Interior gap superfluidity, *Phys. Rev. Lett.* 90(4), 047002 (2003)
7. G. Sarma, On the influence of a uniform exchange field acting on the spins of the conduction electrons in a superconductor, *J. Phys. Chem. Solids* 24(8), 1029 (1963)
8. H. Müther and A. Sedrakian, Spontaneous breaking of rotational symmetry in superconductors, *Phys. Rev. Lett.* 88(25), 252503 (2002)
9. D. E. Sheehy and L. Radzihovsky, BEC–BCS crossover, phase transitions and phase separation in polarized resonantly-paired superfluids, *Ann. Phys.* 322(8), 1790 (2007)
10. G. Orso, Attractive Fermi gases with unequal spin populations in highly elongated traps, *Phys. Rev. Lett.* 98(7), 070402 (2007)
11. H. Hu, X. J. Liu, and P. D. Drummond, Phase diagram of a strongly interacting polarized Fermi gas in one dimension, *Phys. Rev. Lett.* 98(7), 070403 (2007)
12. W. Zhang and W. Yi, Topological Fulde–Ferrell–Larkin–Ovchinnikov states in spin–orbit-coupled Fermi gases, *Nat. Commun.* 4, 2711 (2013)
13. W. Yi, W. Zhang, and X. L. Cui, Pairing superfluidity in spin–orbit coupled ultracold Fermi gases, *Sci. China Phys. Mech. Astron.* 58(1), 014201 (2015)
14. T. K. Koponen, T. Paananen, J. P. Martikainen, M. R. Bakhtiari, and P. Törmä, FFLO state in 1-, 2- and 3-dimensional optical lattices combined with a non-uniform background potential, *New J. Phys.* 10(4), 045014 (2008)
15. Z. Cai, Y. Wang, and C. Wu, Stable Fulde–Ferrell–Larkin–Ovchinnikov pairing states in two-dimensional and three-dimensional optical lattices, *Phys. Rev. A* 83(6), 063621 (2011)
16. Z. Zhang, H. H. Hung, C. M. Ho, E. Zhao, and W. V. Liu, Modulated pair condensate of p-orbital ultracold fermions, *Phys. Rev. A* 82(3), 033610 (2010)
17. S. Yin, J. E. Baarsma, M. O. J. Heikkinen, J. P. Martikainen, and P. Törmä, Superfluid phases of fermions with hybridized s and p orbitals, *Phys. Rev. A* 92(5), 053616 (2015)
18. B. Liu, X. Li, R. G. Hulet, and W. V. Liu, Detecting p-phase superfluids with p-wave symmetry in a quasi-one-dimensional optical lattice, *Phys. Rev. A* 94, 031602(R) (2016)
19. A. I. Buzdin, Proximity effects in superconductor-ferromagnet heterostructures, *Rev. Mod. Phys.* 77(3), 935 (2005) (and references therein)
20. C. Bernhard, J. L. Tallon, C. Niedermayer, T. Blasius, A. Golnik, E. Brücher, R. K. Kremer, D. R. Noakes, C. E. Stronach, and E. J. Ansaldo, Coexistence of ferromagnetism and superconductivity in the hybrid ruthenate-cuprate compound $RuSr_2GdCu_2O_8$ studied by muon spin rotation and dc magnetization, *Phys. Rev. B* 59(21), 14099 (1999)
21. A. C. McLaughlin, W. Zhou, J. P. Attfield, A. N. Fitch, and J. L. Tallon, Structure and microstructure of the ferromagnetic superconductor $RuSr_2GdCu_2O_8$, *Phys. Rev. B* 60(10), 7512 (1999)
22. O. Chmaissem, J. D. Jorgensen, H. Shaked, P. Dollar, and J. L. Tallon, Crystal and magnetic structure of ferromagnetic superconducting $RuSr_2GdCu_2O_8$, *Phys. Rev. B* 61(9), 6401 (2000)
23. I. Zapata, B. Wunsch, N. T. Zinner, and E. Demler, p-phases in balanced fermionic superfluids on spin-dependent optical lattices, *Phys. Rev. Lett.* 105(9), 095301 (2010)
24. I. E. Mooij, T. P. Orlando, L. Levitov, L. Tian, C. H. van der Wal, and S. Lloyd, Josephson persistent-current qubit, *Science* 285(5430), 1036 (1999)
25. L. B. Ioffe, V. B. Geshkenbein, M. V. Feigel'man, A. L. Fauchère, and G. Blatter, Environmentally decoupled *sds*-wave Josephson junctions for quantum computing, *Nature* 398(6729), 679 (1999)
26. T. Müller, S. Fölling, A. Widera, and I. Bloch, State preparation and dynamics of ultracold atoms in higher lattice orbitals, *Phys. Rev. Lett.* 99(20), 200405 (2007)
27. G. Wirth, M. Ölschläger, and A. Hemmerich, Evidence for orbital superfluidity in the P-band of a bipartite optical square lattice, *Nat. Phys.* 7(2), 147 (2011)
28. P. Soltan-Panahi, D. S. Lühmann, J. Struck, P. Windpassinger, and K. Sengstock, Quantum phase transition to unconventional multi-orbital superfluidity in optical lattices, *Nat. Phys.* 8(1), 71 (2011)
29. D. S. Petrov and G. V. Shlyapnikov, Interatomic collisions in a tightly confined Bose gas, *Phys. Rev. A* 64(1), 012706 (2001)
30. J. P. Kestner and L. M. Duan, Effective low-dimensional Hamiltonian for strongly interacting atoms in a transverse trap, *Phys. Rev. A* 76(6), 063610 (2007)
31. W. Zhang, G. D. Lin, and L. M. Duan, BCS–BEC crossover of a quasi-two-dimensional Fermi gas: The significance of dressed molecules, *Phys. Rev. A* 77(6), 063613 (2008)
32. W. Zhang, G. D. Lin, and L. M. Duan, Berezinskii–Kosterlitz–Thouless transition in a trapped quasi-two-dimensional Fermi gas near a Feshbach resonance, *Phys. Rev. A* 78(4), 043617 (2008)
33. S. S. Botelho and C. A. R. Sá de Melo, Vortex-antivortex lattice in ultracold fermionic gases, *Phys. Rev. Lett.* 96(4), 040404 (2006)
34. V. L. Berezinskii, Destruction of long-range order in one-dimensional and two-dimensional systems having a con-tinuous symmetry group (I): Classical systems, *Sov. Phys. JETP* 32, 493 (1971)
35. J. M. Kosterlitz and D. Thouless, Long range order and metastability in two dimensional solids and superfluids. (Application of dislocation theory), *J. Phys. C: Solid State Phys.* 5, L124 (1972)